
Generative models for graph-based protein design

John Ingraham, Vikas K. Garg, Regina Barzilay, Tommi Jaakkola
Computer Science and Artificial Intelligence Lab, MIT
{ingraham, vgarg, regina, tommi}@csail.mit.edu

Abstract

Engineered proteins offer the potential to solve many problems in biomedicine, energy, and materials science, but creating designs that succeed is difficult in practice. A significant aspect of this challenge is the complex coupling between protein sequence and 3D structure, with the task of finding a viable design often referred to as the *inverse protein folding problem*. In this work, we introduce conditional language models for protein sequences that directly condition on a graph specification of the target structure. Our approach efficiently captures the complex dependencies in proteins by focusing on those that are long-range in sequence but local in 3D space. Our framework improves in both speed and reliability over conventional and neural network-based approaches, and takes a step toward rapid and targeted biomolecular design with the aid of deep generative models.

1 Introduction

A central goal for computational protein design is to automate the invention of protein molecules with defined structural and functional properties. This field has seen tremendous progress in the past two decades [1], including the design of novel 3D folds [2], enzymes [3], and complexes [4]. However, the current practice often requires multiple rounds of trial-and-error, with first designs frequently failing [5, 6]. Several of the challenges stem from the bottom-up nature of contemporary approaches that rely on both the accuracy of *energy functions* to describe protein physics as well as on the efficiency of *sampling algorithms* to explore the protein sequence and structure space.

Here, we explore an alternative, top-down framework for protein design that directly learns a conditional generative model for protein *sequences* given a specification of the target structure, which is represented as a *graph* over the residues (amino acids). Specifically, we augment the autoregressive self-attention of recent sequence models [7] with graph-based descriptions of the 3D structure. By composing multiple layers of structured self-attention, our model can effectively capture higher-order, interaction-based dependencies between sequence and structure, in contrast to previous parametric approaches [8, 9] that are limited to only the first-order effects.

The graph-structured conditioning of a sequence model affords several benefits, including favorable computational efficiency, inductive bias, and representational flexibility. We accomplish the first two by leveraging a well-evidenced finding in protein science, namely that long-range dependencies in sequence are generally short-range in 3D space [10–12]. By making the graph and self-attention similarly sparse and localized in 3D space, we achieve computational scaling that is linear in sequence length. Additionally, graph structured inputs offer representational flexibility, as they accommodate both coarse, ‘flexible backbone’ (connectivity and topology) as well as fine-grained (precise atom locations) descriptions of structure.

We demonstrate the merits of our approach via a detailed empirical study. Specifically, we evaluate our model at *structural generalization* to sequences of protein folds that were outside of the training set. For fixed-backbone sequence design, our model achieves considerably improved statistical

performance over a neural-network based model and also achieves higher accuracy and efficiency than Rosetta fixbb, a state-the-art program for protein design.

The rest of the paper is organized as follows. We first position our contributions with respect to the prior work in Section 1.1. We provide details on our methods, including structure representation, in Section 2. We introduce our *Structured Transformer* model in Section 2.2. The details of our experiments are laid out in Section 3, and the corresponding results that elucidate the merits of our approach are presented in Section 4.

1.1 Related Work

Generative models for protein sequence and structure A number of works have explored the use of generative models for protein engineering and design [13]. Recently [8, 9, 14] proposed neural network-based models for sequences given 3D structure, where the amino acids are modeled independently of one another. [15] introduced a generative model for protein sequences conditioned on a 1D, context-free grammar based specification of the fold topology. Multiple works [16, 17] have modeled the conditional distribution of single amino acids given surrounding structure and sequence context with convolutional neural networks. In contrast to these works, our model captures the joint distribution of the full protein sequence while grounding these dependencies in terms of long-range interactions arising from structure.

In parallel to the development of structure-based models, there has been considerable work on deep generative models for protein sequences in individual protein families [18–21]. While useful, these methods presume the availability of a large number of sequences from a particular family, which are unavailable in the case of designing novel proteins that diverge significantly from natural sequences.

Several groups have obtained promising results using (unconditional) protein language models [22–25] to learn sequence representations that transfer well to supervised tasks. While serving different purposes, we emphasize that one advantage of conditional generative modeling is to facilitate adaptation to specific (and potentially novel) parts of structure space. Language models trained on hundreds of millions of evolutionary sequences are nevertheless ‘semantically’ bottlenecked by the much smaller number of evolutionary 3D folds (thousands) that these sequences represent. We propose evaluating protein language models with *structure*-based splitting of sequence data, and begin to see how unconditional language models may struggle to assign high likelihoods to sequences from out-of-training folds.

In a complementary line of research, several deep and differentiable parameterizations of protein structure [26–29] have been recently proposed that could be used to generate, optimize, or validate 3D structures for input to sequence design.

Protein design and interaction graphs For classical approaches to computational protein design, which are based on joint modeling of structure and sequence, we refer the reader to a review of both methods and accomplishments in [1]. Many of the major ‘firsts’ in protein design are due to Rosetta [30, 31], a leading framework for protein design. More recently, there have been successes with non-parametric approaches to protein design [32] that are based on finding substructural homologies between the target and diverse templates in large protein database. We will focus on comparisons to Rosetta, since it is based on a shared parametric energy function that captures the sequence-structure relationship.

Self-Attention Our model extends the Transformer [33] to capture sparse, pairwise relational information between sequence elements. The dense variation of this problem was explored in [34] and [35]. As noted in those works, incorporating general pairwise information incurs $\mathcal{O}(N^2)$ memory (and computational) cost for sequences of length N , which can be highly limiting for training on GPUs. We circumvent this cost by instead restricting the self-attention to the sparsity of the input graph. Given this graph-structured self-attention, our model may also be reasonably cast in the framework of message-passing or graph neural networks [36, 37]. Our approach is similar to Graph Attention Networks [38], but augmented with edge features and an autoregressive decoder.

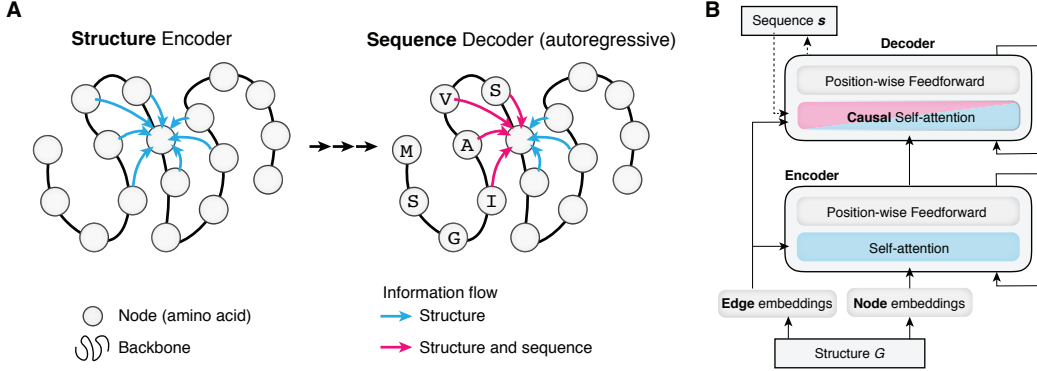


Figure 1: **A graph-based, autoregressive model for protein sequences given 3D structures.** (A) We cast protein design as language modeling conditioned on an input graph. In our architecture, an encoder develops sequence-independent, contextual embeddings of each residue in the 3D structure with multi-head self-attention [7] on the spatial k -nearest neighbors graph. An autoregressive decoder then predicts amino acid s_i given the full structure and previously decoded amino acids. (B) Each layer interleaves local neighborhood aggregation with position-wise feedforward sub-layers.

2 Methods

In this work, we introduce a *Structured Transformer* model that draws inspiration from the self-attention based *Transformer* model [7] and is augmented for scalable incorporation of relational information (Figure 1). While general relational attention incurs quadratic memory and computation costs, we avert these by restricting the attention for each node i to the set $N(i, k)$ of its k -nearest neighbors in 3D space. Since our architecture is multilayered, iterated local attention can derive progressively more global estimates of context for each node i . Second, unlike the standard Transformer, we also include edge features to embed the spatial and positional dependencies in deriving the attention. Thus, our model generalizes Transformer to spatially structured settings.

2.1 Representing structure as a graph

We represent protein structure in terms of an attributed graph $\mathcal{G} = (\mathcal{V}, \mathcal{E})$ with node features $\mathcal{V} = \{v_1, \dots, v_N\}$ describing each residue (amino acid, which are the letters which compose a protein sequence) and edge features $\mathcal{E} = \{e_{ij}\}_{i \neq j}$ capturing relationships between them. This formulation can accommodate different variations on the macromolecular design problem, including both the ‘rigid backbone’ design where the precise coordinates of backbone atoms are fixed, as well as the ‘flexible backbone’ design where softer constraints such as blueprints of hydrogen-bonding connectivity [5] or 1D architectures [15] could define the structure of interest.

3D considerations For a rigid-body design problem, the structure for conditioning is a fixed set of backbone coordinates $\mathcal{X} = \{x_i \in \mathbb{R}^3 : 1 \leq i \leq N\}$, where N is the number of positions¹. We desire a graph representation of the coordinates $\mathcal{G}(\mathcal{X})$ that has two properties:

- *Invariance.* The features are invariant to rotations and translations.
- *Locally informative.* The edge features incident to v_i due to its neighbors $N(i, k)$, i.e. $\{e_{ij}\}_{j \in N(i, k)}$, contain sufficient information to reconstruct all adjacent coordinates $\{x_j\}_{j \in N(i, k)}$ up to rigid-body motion.

While invariance is motivated by standard symmetry considerations, the second property is motivated by limitations of current graph neural networks [36]. In these networks, updates to node features v_i depend only on the edge and node features adjacent to v_i . However, typically, these features are

¹Here we consider a single representative coordinate per position when deriving edge features but may revisit multiple atom types per position for features such as backbone angles or hydrogen bonds.

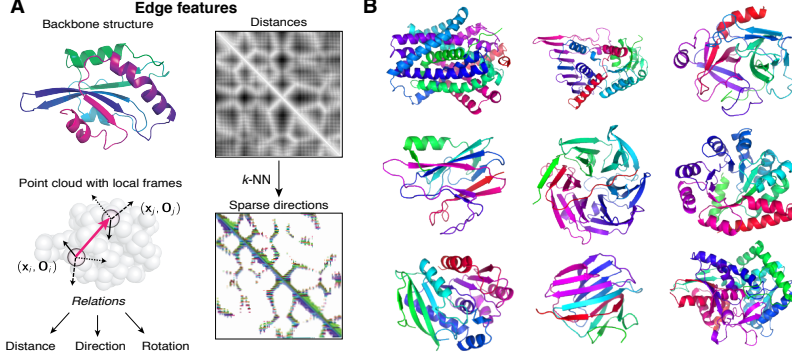


Figure 2: **Spatial features capture structural relationships across diverse folds.** (A) For rigid-body protein design, we develop spatial relations based on the relative distances, directions, and orientations between local reference frames $(\mathbf{x}_i, \mathbf{O}_i)$ and $(\mathbf{x}_j, \mathbf{O}_j)$ at different positions in the protein backbone. We achieve efficient scaling to large proteins by computing a k -Nearest Neighbors graph from Euclidean distances (right, top) and restrict all subsequent computation, such as relative directions (right, bottom), to this graph. (B) Example of topological variation in the dataset. Protein chains in train, test, and validation are split by the sub-chain CATH [40] topologies, which means that folds in each set will have distinct 2D patterns of connectivity.

insufficient to reconstruct the relative neighborhood positions $\{\mathbf{x}_j\}_{j \in \mathcal{N}(i,k)}$, so individual updates cannot fully depend on the ‘local environment’. For example, pairwise distances D_{ij} and D_{il} are insufficient to determine if \mathbf{x}_j and \mathbf{x}_l are on the same or opposite sides of \mathbf{x}_i .

Relative spatial encodings We develop invariant and locally informative features by first augmenting the points \mathbf{x}_i with ‘orientations’ \mathbf{O}_i that define a local coordinate system at each point (Figure 2). We define these in terms of the backbone geometry as

$$\mathbf{O}_i = [\mathbf{b}_i \quad \mathbf{n}_i \quad \mathbf{b}_i \times \mathbf{n}_i],$$

where \mathbf{b}_i is the negative bisector of angle between the rays $(\mathbf{x}_{i-1} - \mathbf{x}_i)$ and $(\mathbf{x}_{i+1} - \mathbf{x}_i)$, and \mathbf{n}_i is a unit vector normal to that plane. Formally, we have

$$\mathbf{u}_i = \frac{\mathbf{x}_i - \mathbf{x}_{i-1}}{\|\mathbf{x}_i - \mathbf{x}_{i-1}\|}, \quad \mathbf{b}_i = \frac{\mathbf{u}_i - \mathbf{u}_{i+1}}{\|\mathbf{u}_i - \mathbf{u}_{i+1}\|}, \quad \mathbf{n}_i = \frac{\mathbf{u}_i \times \mathbf{u}_{i+1}}{\|\mathbf{u}_i \times \mathbf{u}_{i+1}\|}.$$

Finally, we derive the spatial edge features $e_{ij}^{(s)}$ from the rigid body transformation that relates reference frame $(\mathbf{x}_i, \mathbf{O}_i)$ to reference frame $(\mathbf{x}_j, \mathbf{O}_j)$. While this transformation has 6 degrees of freedom, we decompose it into features for distance, direction, and orientation as

$$e_{ij}^{(s)} = \left(\mathbf{r}(\|\mathbf{x}_j - \mathbf{x}_i\|), \quad \mathbf{O}_i^T \frac{\mathbf{x}_j - \mathbf{x}_i}{\|\mathbf{x}_j - \mathbf{x}_i\|}, \quad \mathbf{q}(\mathbf{O}_i^T \mathbf{O}_j) \right).$$

Here the first vector is a *distance* encoding $\mathbf{r}(\cdot)$ lifted into a radial basis², the second vector is a *direction* encoding that corresponds to the relative direction of \mathbf{x}_j in the reference frame of $(\mathbf{x}_i, \mathbf{O}_i)$, and the third vector is an *orientation* encoding $\mathbf{q}(\cdot)$ of the quaternion representation of the spatial rotation matrix $\mathbf{O}_i^T \mathbf{O}_j$. Quaternions represent 3D rotations as four-element vectors that can be efficiently and reasonably compared by inner products [39].³

Relative positional encodings Taking a cue from the original Transformer model, we obtain positional embeddings $e_{ij}^{(p)}$ that encode the role of local structure around node i . Specifically, we need to model the positioning of each neighbor j relative to the node under consideration i . Therefore, we obtain the position embedding as a sinusoidal function of the gap $i - j$. We retain the sign of

²We used 16 Gaussian RBFs isotropically spaced from 0 to 20 Angstroms.

³We represent quaternions in terms of their vector of real coefficients.

the distance $i - j$ because protein backbones are asymmetric. These relative distances contrast the absolute positional encodings of the original Transformer, and instead matches the relative encodings in [34].

Node and edge features Finally, we obtain an aggregate edge encoding vector e_{ij} by concatenating the structural encodings $e_{ij}^{(s)}$ and the positional encodings $e_{ij}^{(p)}$ and then linearly transforming them to have the same dimension as the model. We only include edges in the k -nearest neighbors graph of \mathcal{X} , with $k = 30$ for all experiments. This k is generous, as typical definitions of residue-residue contacts in proteins will result in < 20 contacts per residue. For node features, we compute the three dihedral angles of the protein backbone $(\phi_i, \psi_i, \omega_i)$ and embed these on the 3-torus as $\{\sin, \cos\} \times (\phi_i, \psi_i, \omega_i)$.

Flexible backbone features We also consider 'flexible backbone' descriptions of 3D structure based on topological binary edge features and coarse backbone geometry. We combine the relative positional encodings with two binary edge features: *contacts* that indicate when the distance between C_α residues at i and j are less than 8 Angstroms and *hydrogen bonds* which are directed and defined by the electrostatic model of DSSP [41]. For coarse node features, we compute virtual dihedral angles and bond angles between backbone C_α residues, interpret them as spherical coordinates, and represent them as points on the unit sphere.

2.2 Structured Transformer

Autoregressive decomposition We decompose the joint distribution of the sequence given structure $p(\mathbf{s}|\mathbf{x})$ autoregressively as

$$p(\mathbf{s}|\mathbf{x}) = \prod_i p(s_i|\mathbf{x}, \mathbf{s}_{<i}),$$

where the conditional probability $p(s_i|\mathbf{x}, \mathbf{s}_{<i})$ of amino acid s_i at position i is conditioned on both the input structure \mathbf{x} and the preceding amino acids $\mathbf{s}_{<i} = \{s_1, \dots, s_{i-1}\}$.⁴ These conditionals are parameterized in terms of two sub-networks: an *encoder* that computes refined node embeddings from structure-based node features $\mathcal{V}(\mathbf{x})$ and edge features $\mathcal{E}(\mathbf{x})$ and a *decoder* that autoregressively predicts letter s_i given the preceding sequence and structural embeddings from the encoder (Figure 1).

Encoder Our encoder module is designed as follows. A transformation $\mathbf{W}_h : \mathbb{R}^{d_v} \mapsto \mathbb{R}^d$ produces initial embeddings $\mathbf{h}_i = \mathbf{W}_h(\mathbf{v}_i)$ from the node features \mathbf{v}_i pertaining to position $i \in [N] \triangleq \{1, 2, \dots, N\}$.

Each layer of the encoder implements a multi-head self-attention component, where head $\ell \in [L]$ can attend to a separate subspace of the embeddings via learned query, key and value transformations [7]. The queries are derived from the current embedding at node i while the keys and values from the relational information $\mathbf{r}_{ij} = (\mathbf{h}_j, \mathbf{e}_{ij})$ at adjacent nodes $j \in N(i, k)$. Specifically, $\mathbf{W}_q^{(\ell)}$ maps \mathbf{h}_i to *query* embeddings $\mathbf{q}_i^{(\ell)}$, $\mathbf{W}_z^{(\ell)}$ maps pairs \mathbf{r}_{ij} to *key* embeddings $\mathbf{z}_{ij}^{(\ell)}$ for $j \in N(i, k)$, and $\mathbf{W}_v^{(\ell)}$ maps the same pairs \mathbf{r}_{ij} to *value* embeddings $\mathbf{v}_{ij}^{(\ell)}$ for each $i \in [N], \ell \in [L]$. Decoupling the mappings for keys and values allows each to depend on different subspaces of the representation.

We compute the attention $a_{ij}^{(\ell)}$ between query $\mathbf{q}_i^{(\ell)}$ and key $\mathbf{z}_{ij}^{(\ell)}$ as a function of their scaled inner product:

$$a_{ij}^{(\ell)} = \frac{\exp(m_{ij}^{(\ell)})}{\sum_{j' \in N(i, k)} \exp(m_{ij'}^{(\ell)})}, \quad \text{where } m_{ij}^{(\ell)} = \frac{\mathbf{q}_i^{(\ell)\top} \mathbf{z}_{ij}^{(\ell)}}{\sqrt{d}}.$$

The results of each attention head ℓ are collected as the weighted sum

$$\mathbf{h}_i^{(\ell)} = \sum_{j \in N(i, k)} a_{ij}^{(\ell)} \mathbf{v}_{ij}^{(\ell)},$$

⁴We anticipate that alternative orderings for decoding the sequence may be favorable but leave this to future work.

Table 1: **Null perplexities** for common statistical models of proteins.

Null model	Perplexity	Conditioned on
Uniform	20.00	-
Natural frequencies	17.83	Random position in a natural protein
Pfam HMM profiles	11.64	Specific position in a specific protein family

and then concatenated and transformed to give the update

$$\Delta \mathbf{h}_i = \mathbf{W}_o \text{Concat} \left(\mathbf{h}_i^{(1)}, \dots, \mathbf{h}_i^{(L)} \right).$$

We update the embeddings with this residual, and alternate between these self-attention layers and position-wise feedforward layers as in the original Transformer [7]. We stack multiple layers atop each other, and thereby obtain continually refined embeddings as we traverse the layers bottom up. The encoder yields the embeddings produced by the topmost layer as its output.

Decoder Our decoder module has the same structure as the encoder but with augmented relational information \mathbf{r}_{ij} that allows access to the preceding sequence elements $\mathbf{s}_{<i}$ in a *causally consistent* manner. In contrast to the encoder, where the keys and values are based on the relational information $\mathbf{r}_{ij} = (\mathbf{h}_j, \mathbf{e}_{ij})$, the decoder can additionally access sequence elements \mathbf{s}_j as

$$\mathbf{r}_{ij}^{(\text{dec})} = \begin{cases} (\mathbf{h}_j^{(\text{dec})}, \mathbf{e}_{ij}, \mathbf{g}(\mathbf{s}_j)) & i > j \\ (\mathbf{h}_j^{(\text{enc})}, \mathbf{e}_{ij}, \mathbf{0}) & i \leq j \end{cases}.$$

Here $\mathbf{h}_j^{(\text{dec})}$ is the embedding of node j in the current layer of the decoder, $\mathbf{h}_j^{(\text{enc})}$ is the embedding of node j in the final layer of the encoder, and $\mathbf{g}(\mathbf{s}_j)$ is a sequence embedding of amino acid \mathbf{s}_j at node j . This concatenation and masking structure ensures that sequence information only flows to position i from positions $j < i$, but still allows position i to attend to subsequent structural information unlike the standard Transformer decoder.

We now demonstrate the merits of our approach via a detailed empirical analysis. We begin with the experimental set up including our architecture, and description of the data used in our experiments.

3 Training

Architecture In all experiments, we used three layers of self-attention and position-wise feedforward modules for the encoder and decoder with a hidden dimension of 128.

Optimization We trained models using the learning rate schedule and initialization of the original Transformer paper [7], a dropout rate of 10% [42], a label smoothing rate of 10%, and early stopping based on validation perplexity. The unconditional language models did not include dropout or label smoothing.

Dataset To evaluate the ability of our models to generalize across different protein folds, we collected a dataset based on the CATH hierarchical classification of protein structure [40]. For all domains in the CATH 4.2 40% non-redundant set of proteins, we obtained full chains up to length 500 and then randomly assigned their CATH topology classifications (CAT codes) to train, validation and test sets at a targeted 80/10/10 split. Since each chain can contain multiple CAT codes, we first removed any redundant entries from train and then from validation. Finally, we removed any chains from the test set that had CAT overlap with train and removed chains from the validation set with CAT overlap to train or test. This resulted in a dataset of 18024 chains in the training set, 608 chains in the validation set, and 1120 chains in the test set. There is zero CAT overlap between these sets.

4 Results

A challenge in evaluating computational protein design methods is the *degeneracy* of the relationship between protein structure and sequence. Many protein sequences may reasonably design the same

Table 2: **Per-residue perplexities for protein language modeling** (lower is better). The protein chains have been cluster-split by CATH topology, such that test includes only unseen 3D folds. While a structure-conditioned language model can generalize in this structure-split setting, unconditional language models struggle.

Test set	Short	Single chain	All
Structure-conditioned models			
Structured Transformer (ours)	8.54	9.03	6.85
SPIN2 [8]	12.11	12.61	-
Language models			
LSTM ($h = 128$)	16.06	16.38	17.13
LSTM ($h = 256$)	16.08	16.37	17.12
LSTM ($h = 512$)	15.98	16.38	17.13
Test set size	94	103	1120

3D structure [43], meaning that sequence similarity need not necessarily be high. At the same time, single mutations may cause a protein to break or misfold, meaning that high sequence similarity isn’t sufficient for a correct design. To deal with this, we will focus on three kinds of evaluation: (i) likelihood-based, where we test the ability of the generative model to give high likelihood to held out sequences, (ii) native sequence recovery, where we evaluate generated sequences vs the native sequences of templates, and (iii) experimental comparison, where we compare the likelihoods of the model to high-throughput data from a de novo protein design experiment.

We find that our model is able to attain considerably improved statistical performance in its likelihoods while simultaneously providing more accurate and efficient sequence recovery.

4.1 Statistical comparison to likelihood-based models

Protein perplexities What kind of perplexities might be useful? To provide context, we first present perplexities for some simple models of protein sequences in Table 1. The amino acid alphabet and its natural frequencies upper-bound perplexity at 20 and ~ 17.8 , respectively. Random protein sequences under these null models are unlikely to be functional without further selection [44]. First order profiles of protein sequences such as those from the Pfam database [45], however, are widely used for protein engineering. We found the average perplexity per letter of profiles in Pfam 32 (ignoring alignment uncertainty) to be ~ 11.6 . This suggests that even models with high perplexities of this order have the potential to be useful models for the space of functional protein sequences.

The importance of structure We found that there was a significant gap between unconditional language models of protein sequences and models conditioned on structure. Remarkably, for a range of structure-independent language models, the typical test perplexities are ~ 16 -17 (Table 2), which were barely better than null letter frequencies (Table 1). We emphasize that the RNNs were not broken and could still learn the training set in these capacity ranges. All structure-based models had (unsurprisingly) considerably lower perplexities. In particular, our Structured Transformer model attained a perplexity of ~ 7 on the full test set. It would seem that protein language models trained on one subset of 3D folds (in our cluster-splitting procedure) generalize poorly to predict the sequences

Table 3: **Ablation of graph features and model components.** Test perplexities (lower is better).

Node features	Edge features	Aggregation	Short	Single chain	All
Rigid backbone					
Dihedrals	Distances, Orientations	Attention	8.54	9.03	6.85
Dihedrals	Distances, Orientations	PairMLP	8.33	8.86	6.55
C_α angles	Distances, Orientations	Attention	9.16	9.37	7.83
Dihedrals	Distances	Attention	9.11	9.63	7.87
Flexible backbone					
C_α angles	Contacts, Hydrogen bonds	Attention	11.71	11.81	11.51

Method	Recovery (%)	Speed (AA/s) CPU	Speed (AA/s) GPU
Rosetta 3.10 fixbb	18.1	4.88×10^{-1}	N/A
Ours ($T = 0.1$)	27.6	2.22×10^2	1.04×10^4

(a) Single chain test set

Method	Recovery (%)
Rosetta, fixbb 1	33.1
Rosetta, fixbb 2	38.4
Ours ($T = 0.1$)	39.2 ± 0.1

(b) Ollikainen 40 benchmark

Table 4: **Improved reliability and speed compared to Rosetta.** (a) Our model more accurately recovers native sequences than Rosetta fixbb (median recovery across 103 templates, 100 designs per) with greater speed (CPU: single core of Intel Xeon Gold 5115, GPU: NVIDIA RTX 2080). This set includes traditionally difficult templates based on NMR structures. (b) Evaluation with a prior benchmark of 40 structures, 100 designs per structure. Average of 4 trials ± 2 standard deviations.

of unseen folds, which is important to consider when training protein language models for protein engineering and design.

Improvement over deep profile-based methods We also compared to a recent method SPIN2 that predicts, using deep neural networks, protein sequence profiles given protein structures [8]. Since SPIN2 is computationally intensive (minutes per protein for small proteins) and was trained on complete proteins rather than chains, we evaluated it on two subsets of the full test set: a ‘Small’ subset of the test set containing chains up to length 100 and a ‘Single chain’ subset containing only those models where the single chain accounted for the entire protein record in the Protein Data Bank. Both subsets discarded any chains with structural gaps (chain break). We found that our Structured Transformer model significantly improved upon the perplexities of SPIN2 (Table 2).

Graph representations and attention mechanisms The graph-based formulation of protein design can accommodate very different formulations of the problem depending on how structure is represented by a graph. We tested different approaches for representing the protein including both more ‘rigid’ design with precise geometric details, and ‘flexible’ topological design based on spatial contacts and hydrogen bonding (Table 3). For the best perplexities, we found that using local orientation information was indeed important above simple distance measures. At the same time, even the topological features were sufficient to obtain better perplexities than SPIN2 (Table 2), which uses precise atomic details.

In addition to varying the graph features, we also experimented with an alternative aggregation function from message passing neural networks [36].⁵ We found that a simple aggregation function $\Delta \mathbf{h}_i = \sum_j \text{MLP}(\mathbf{h}_j, \mathbf{h}_j, \mathbf{e}_{ij})$ led to the best performance of all models, where $\text{MLP}(\cdot)$ is a two layer perceptron that preserves the hidden dimension of the model. We speculate that this is due to potential overfitting by the attention mechanism. Although all following experiments still use multi-head self-attention and full rigid backbone features, this suggests room future improvements.

4.2 Benchmarking protein redesign

Decoding strategies Generating protein sequence designs requires a sampling scheme for drawing high-likelihood sequences from the model. While beam-search or top- k sampling [46] are commonly used heuristics for decoding, we found that simple biased sampling from the temperature adjusted distributions $p^{(T)}(\mathbf{s}|\mathbf{x}) = \prod_i \frac{p(s_i|\mathbf{x}, \mathbf{s}_{<i})^{1/T}}{\sum_a p(a|\mathbf{x}, \mathbf{s}_{<i})^{1/T}}$ was sufficient for obtaining sequences with higher likelihoods than native. We used a temperature of $T = 0.1$ selected from sequence recovery on validation. For conditional redesign of a subset of positions in a protein, we speculate that the likelihood calculation is sufficiently fast such that MCMC-based approaches such as Gibbs sampling may be feasible.

⁵We thank one of our reviewers for this suggestion.

Table 5: **Structure-conditioned likelihoods correlate with mutation effects in *de novo*-designed miniproteins.** Shown are Pearson correlation coefficients (R , higher is better) between the log-likelihoods of mutated sequences and high-throughput mutation effect data from a systematic design of miniproteins [6]. Each design (column) includes 775 experimentally tested mutant protein sequences.

Design	$\beta\beta\alpha\beta\beta_{37}$	$\beta\beta\alpha\beta\beta_{1498}$	$\beta\beta\alpha\beta\beta_{1702}$	$\beta\beta\alpha\beta\beta_{1716}$	$\alpha\beta\beta\alpha_{779}$
Rigid backbone	0.47	0.45	0.12	0.47	0.57
Flexible backbone	0.50	0.44	0.17	0.40	0.56

Design	$\alpha\beta\beta\alpha_{223}$	$\alpha\beta\beta\alpha_{726}$	$\alpha\beta\beta\alpha_{872}$	$\alpha\alpha\alpha_{134}$	$\alpha\alpha\alpha_{138}$
Rigid backbone	0.36	0.11	0.21	0.24	0.33
Flexible backbone	0.33	0.21	0.23	0.36	0.41

Comparison to Rosetta To evaluate the performance of our model at generating realistic protein sequences, we performed two experiments that compare with Rosetta [30], a state-of-the-art framework for computational protein design. We found that our model was more accurate and significantly faster than Rosetta (Table 4). In the first, we used the latest version of Rosetta (3.10) to design sequences for our ‘Single chain’ test set with the *fixbb* fixed-backbone design protocol and default parameters (Table 4, a). In the second, we also compared to a prior benchmark from members of the Rosetta community [47, 48] across 40 diverse proteins. For this set of proteins, we re-split our dataset to form new training and validation sets with no CAT overlap to the 40 templates for design. Although this reduced the size of the training set from $\sim 18,000$ to $\sim 10,000$ chains, we found our model to be both more accurate than and several orders of magnitude faster than Rosetta (Table 4, b).

4.3 Unsupervised anomaly detection for experimental protein design

While synthesis and testing of designed sequences is the gold standard of evaluating protein design methods we can measure what our structure-conditioned language model ‘knows’ about protein function by comparing the likelihoods it assigns to functional and non-functional mutant proteins from recent high-throughput design experiments as a kind of *unsupervised anomaly detection* [18]. We compare to a recent high-throughput design and mutagenesis experiment in which several *de novo* designed mini-proteins were subject to systematic mutagenesis to all possible point mutations [6]. We find that the log-likelihoods of our model non-trivially reflect mutational preferences of designed proteins (Table 5). Importantly, we see that the performance is not dependent on precise 3D geometric features (e.g. distances and orientations) but can also be realized with coarse information (e.g. contacts, hydrogen bonds, and coarse backbone angles).

5 Conclusion

We presented a new deep generative model to ‘design’ protein sequences given a graph specification of their structure. Our model augments the traditional sequence-level self-attention of Transformers [7] with relational 3D structural encodings and is able to leverage the spatial locality of dependencies in molecular structures for efficient computation. When evaluated on unseen folds, the model achieves significantly improved perplexities over recent neural network-based generative models and more accurate and efficient sequence generation than the state-of-art program Rosetta.

Our framework suggests the possibility of being able to efficiently design and engineer protein sequences with structurally-guided deep generative models, and underscores the central role of modeling sparse long-range dependencies in biological sequences.

Acknowledgments

We thank members of the MIT MLPDS consortium, the MIT NLP group, and the reviewers for helpful feedback. This work was supported by the Machine Learning for Pharmaceutical Discovery and Synthesis (MLPDS) consortium.

References

- [1] Po-Ssu Huang, Scott E Boyken, and David Baker. The coming of age of de novo protein design. *Nature*, 537(7620):320, 2016.
- [2] Brian Kuhlman, Gautam Dantas, Gregory C Ireton, Gabriele Varani, Barry L Stoddard, and David Baker. Design of a novel globular protein fold with atomic-level accuracy. *science*, 302(5649):1364–1368, 2003.
- [3] Justin B Siegel, Alexandre Zanghellini, Helena M Lovick, Gert Kiss, Abigail R Lambert, Jennifer L St Clair, Jasmine L Gallaher, Donald Hilvert, Michael H Gelb, Barry L Stoddard, et al. Computational design of an enzyme catalyst for a stereoselective bimolecular diels-alder reaction. *Science*, 329(5989):309–313, 2010.
- [4] Jacob B Bale, Shane Gonen, Yuxi Liu, William Sheffler, Daniel Ellis, Chantz Thomas, Duilio Cascio, Todd O Yeates, Tamir Gonen, Neil P King, et al. Accurate design of megadalton-scale two-component icosahedral protein complexes. *Science*, 353(6297):389–394, 2016.
- [5] Nobuyasu Koga, Rie Tatsumi-Koga, Gaohua Liu, Rong Xiao, Thomas B Acton, Gaetano T Montelione, and David Baker. Principles for designing ideal protein structures. *Nature*, 491(7423):222, 2012.
- [6] Gabriel J Rocklin, Tamuka M Chidyausiku, Inna Goreschnik, Alex Ford, Scott Houliston, Alexander Lemak, Lauren Carter, Rashmi Ravichandran, Vikram K Mulligan, Aaron Chevalier, et al. Global analysis of protein folding using massively parallel design, synthesis, and testing. *Science*, 357(6347):168–175, 2017.
- [7] Ashish Vaswani, Noam Shazeer, Niki Parmar, Jakob Uszkoreit, Llion Jones, Aidan N Gomez, Łukasz Kaiser, and Illia Polosukhin. Attention is all you need. In *Advances in Neural Information Processing Systems*, pages 5998–6008, 2017.
- [8] James O’Connell, Zhixiu Li, Jack Hanson, Rhys Heffernan, James Lyons, Kuldip Paliwal, Abdollah Dehzeni, Yuedong Yang, and Yaoqi Zhou. Spin2: Predicting sequence profiles from protein structures using deep neural networks. *Proteins: Structure, Function, and Bioinformatics*, 86(6):629–633, 2018.
- [9] Jingxue Wang, Huali Cao, John ZH Zhang, and Yifei Qi. Computational protein design with deep learning neural networks. *Scientific reports*, 8(1):6349, 2018.
- [10] Debora S Marks, Lucy J Colwell, Robert Sheridan, Thomas A Hopf, Andrea Pagnani, Riccardo Zecchina, and Chris Sander. Protein 3d structure computed from evolutionary sequence variation. *PloS one*, 6(12):e28766, 2011.
- [11] Faruck Morcos, Andrea Pagnani, Bryan Lunt, Arianna Bertolino, Debora S Marks, Chris Sander, Riccardo Zecchina, José N Onuchic, Terence Hwa, and Martin Weigt. Direct-coupling analysis of residue coevolution captures native contacts across many protein families. *Proceedings of the National Academy of Sciences*, 108(49):E1293–E1301, 2011.
- [12] Sivaraman Balakrishnan, Hetunandan Kamisetty, Jaime G Carbonell, Su-In Lee, and Christopher James Langmead. Learning generative models for protein fold families. *Proteins: Structure, Function, and Bioinformatics*, 79(4):1061–1078, 2011.
- [13] Kevin K Yang, Zachary Wu, and Frances H Arnold. Machine learning in protein engineering. *arXiv preprint arXiv:1811.10775*, 2018.
- [14] Sheng Chen, Zhe Sun, Yutong Lu, Huiying Zhao, and Yuedong Yang. To improve protein sequence profile prediction through image captioning on pairwise residue distance map. *bioRxiv*, page 628917, 2019.
- [15] Joe G Greener, Lewis Moffat, and David T Jones. Design of metalloproteins and novel protein folds using variational autoencoders. *Scientific reports*, 8(1):16189, 2018.
- [16] Wouter Boomsma and Jes Frelsen. Spherical convolutions and their application in molecular modelling. In *Advances in Neural Information Processing Systems*, pages 3433–3443, 2017.
- [17] Maurice Weiler, Mario Geiger, Max Welling, Wouter Boomsma, and Taco Cohen. 3d steerable cnns: Learning rotationally equivariant features in volumetric data. In *Advances in Neural Information Processing Systems*, pages 10402–10413, 2018.
- [18] Adam J Riesselman, John B Ingraham, and Debora S Marks. Deep generative models of genetic variation capture the effects of mutations. *Nat. Methods*, 15:816–822, 2018.
- [19] Sam Sinai, Eric Kelsic, George M Church, and Martin A Nowak. Variational auto-encoding of protein sequences. *arXiv preprint arXiv:1712.03346*, 2017.

- [20] Jérôme Tubiana, Simona Cocco, and Rémi Monasson. Learning protein constitutive motifs from sequence data. *arXiv preprint arXiv:1803.08718*, 2018.
- [21] Adam J Riesselman, Jung-Eun Shin, Aaron W Kollasch, Conor McMahon, Elana Simon, Chris Sander, Aashish Manglik, Andrew C Kruse, and Debora S Marks. Accelerating protein design using autoregressive generative models. *bioRxiv*, page 757252, 2019.
- [22] Tristan Bepler and Bonnie Berger. Learning protein sequence embeddings using information from structure. In *International Conference on Learning Representations*, 2019.
- [23] Ethan C Alley, Grigory Khimulya, Surojit Biswas, Mohammed AlQuraishi, and George M Church. Unified rational protein engineering with sequence-only deep representation learning. *bioRxiv*, page 589333, 2019.
- [24] Michael Heinzinger, Ahmed Elnaggar, Yu Wang, Christian Dallago, Dmitrii Nachaev, Florian Matthes, and Burkhard Rost. Modeling the language of life-deep learning protein sequences. *bioRxiv*, page 614313, 2019.
- [25] Alexander Rives, Siddharth Goyal, Joshua Meier, Demi Guo, Myle Ott, C. Lawrence Zitnick, Jerry Ma, and Rob Fergus. Biological structure and function emerge from scaling unsupervised learning to 250 million protein sequences. *bioRxiv*, 2019.
- [26] Namrata Anand and Possu Huang. Generative modeling for protein structures. In *Advances in Neural Information Processing Systems*, pages 7505–7516, 2018.
- [27] Namrata Anand, Raphael Eguchi, and Po-Ssu Huang. Fully differentiable full-atom protein backbone generation. 2019.
- [28] John Ingraham, Adam Riesselman, Chris Sander, and Debora Marks. Learning protein structure with a differentiable simulator. In *International Conference on Learning Representations*, 2019.
- [29] Mohammed AlQuraishi. End-to-end differentiable learning of protein structure. *bioRxiv*, page 265231, 2018.
- [30] Andrew Leaver-Fay, Michael Tyka, Steven M Lewis, Oliver F Lange, James Thompson, Ron Jacak, Kristian W Kaufman, P Douglas Renfrew, Colin A Smith, Will Sheffler, et al. Rosetta3: an object-oriented software suite for the simulation and design of macromolecules. In *Methods in enzymology*, volume 487, pages 545–574. Elsevier, 2011.
- [31] Rebecca F Alford, Andrew Leaver-Fay, Jeliasko R Jeliaskov, Matthew J O’Meara, Frank P DiMaio, Hahnbeom Park, Maxim V Shapovalov, P Douglas Renfrew, Vikram K Mulligan, Kalli Kappel, et al. The rosetta all-atom energy function for macromolecular modeling and design. *Journal of chemical theory and computation*, 13(6):3031–3048, 2017.
- [32] Jianfu Zhou, Alexandra E Panaitiu, and Gevorg Grigoryan. A general-purpose protein design framework based on mining sequence-structure relationships in known protein structures. *bioRxiv*, page 431635, 2018.
- [33] Surojit Biswas, Gleb Kuznetsov, Pierce J Ogden, Nicholas J Conway, Ryan P Adams, and George M Church. Toward machine-guided design of proteins. *bioRxiv*, page 337154, 2018.
- [34] Peter Shaw, Jakob Uszkoreit, and Ashish Vaswani. Self-attention with relative position representations. In *Proceedings of the 2018 Conference of the North American Chapter of the Association for Computational Linguistics: Human Language Technologies, Volume 2 (Short Papers)*, volume 2, pages 464–468, 2018.
- [35] Cheng-Zhi Anna Huang, Ashish Vaswani, Jakob Uszkoreit, Noam Shazeer, Curtis Hawthorne, Andrew M Dai, Matthew D Hoffman, and Douglas Eck. An improved relative self-attention mechanism for transformer with application to music generation. *arXiv preprint arXiv:1809.04281*, 2018.
- [36] Justin Gilmer, Samuel S Schoenholz, Patrick F Riley, Oriol Vinyals, and George E Dahl. Neural message passing for quantum chemistry. In *Proceedings of the 34th International Conference on Machine Learning-Volume 70*, pages 1263–1272. JMLR. org, 2017.
- [37] Peter W Battaglia, Jessica B Hamrick, Victor Bapst, Alvaro Sanchez-Gonzalez, Vinicius Zambaldi, Mateusz Malinowski, Andrea Tacchetti, David Raposo, Adam Santoro, Ryan Faulkner, et al. Relational inductive biases, deep learning, and graph networks. *arXiv preprint arXiv:1806.01261*, 2018.
- [38] Petar Veličković, Guillem Cucurull, Arantxa Casanova, Adriana Romero, Pietro Lio, and Yoshua Bengio. Graph attention networks. *arXiv preprint arXiv:1710.10903*, 2017.

- [39] Du Q Huynh. Metrics for 3d rotations: Comparison and analysis. *Journal of Mathematical Imaging and Vision*, 35(2):155–164, 2009.
- [40] Christine A Orengo, AD Michie, S Jones, David T Jones, MB Swindells, and Janet M Thornton. Cath—a hierarchic classification of protein domain structures. *Structure*, 5(8):1093–1109, 1997.
- [41] Wolfgang Kabsch and Christian Sander. Dictionary of protein secondary structure: pattern recognition of hydrogen-bonded and geometrical features. *Biopolymers*, 22(12):2577–2637, 1983.
- [42] Nitish Srivastava, Geoffrey Hinton, Alex Krizhevsky, Ilya Sutskever, and Ruslan Salakhutdinov. Dropout: a simple way to prevent neural networks from overfitting. *The Journal of Machine Learning Research*, 15(1):1929–1958, 2014.
- [43] Hao Li, Robert Helling, Chao Tang, and Ned Wingreen. Emergence of preferred structures in a simple model of protein folding. *Science*, 273(5275):666–669, 1996.
- [44] Anthony D Keefe and Jack W Szostak. Functional proteins from a random-sequence library. *Nature*, 410(6829):715, 2001.
- [45] Sara El-Gebali, Jaina Mistry, Alex Bateman, Sean R Eddy, Aurélien Luciani, Simon C Potter, Matloob Qureshi, Lorna J Richardson, Gustavo A Salazar, Alfredo Smart, et al. The pfam protein families database in 2019. *Nucleic acids research*, 47(D1):D427–D432, 2018.
- [46] Angela Fan, Mike Lewis, and Yann Dauphin. Hierarchical neural story generation. *arXiv preprint arXiv:1805.04833*, 2018.
- [47] Noah Ollikainen and Tanja Kortemme. Computational protein design quantifies structural constraints on amino acid covariation. *PLoS computational biology*, 9(11):e1003313, 2013.
- [48] Shane Ó Conchúir, Kyle A Barlow, Roland A Pache, Noah Ollikainen, Kale Kundert, Matthew J O’Meara, Colin A Smith, and Tanja Kortemme. A web resource for standardized benchmark datasets, metrics, and rosetta protocols for macromolecular modeling and design. *PLOS one*, 10(9):e0130433, 2015.